Free-Space Communications Enabled by Quantum Cascade Lasers

(article starts on next page)

Free-Space Communications Enabled by Quantum Cascade Lasers

Xiaodan Pang,* Oskars Ozolins, Lu Zhang, Richard Schatz, Aleksejs Udalcovs, Xianbin Yu, Gunnar Jacobsen, Sergei Popov, Jiajia Chen, and Sebastian Lourdudoss

Future generations of wireless communication systems are expected to support orders of magnitude faster data transfer with much lower latency than the currently deployed solutions. Development of wireless transceivers of higher bandwidth, low energy consumption, and small footprint becomes challenging with radio frequency (RF) electronic technologies. Photonics-assisted technologies show many advantages in generating signals of ultrabroad bandwidth at high carrier frequencies in the millimeter-wave, terahertz, and IR bands. Among these frequency options, the mid-IR band has recently attracted great interest for future wireless communication due to its intrinsic merits of low propagation loss and high tolerance of atmospheric perturbations. A promising source for mid-IR free-space communications is the semiconductor quantum cascade laser (QCL), which can be directly modulated at a high speed and facilitates monolithic integration for compact transceivers. Herein, the research and development of QCL-based free-space communications are reviewed and a recent experimental study of multigigabit transmission with a directly modulated mid-IR QCL and a commercial off-the-shelf IR photodetector is reported on. Up to 4 Gb s^{-1} transmission of two advanced modulation formats, namely, four-level pulse amplitude modulation (PAM-4) and discrete multitone (DMT) modulation, is demonstrated.

1. Introduction

Semiconductor lasers are playing an important role in the information and communication infrastructure worldwide. Since about three decades ago, the world has witnessed a rapid replacement of copper-wire communication with fiber optics in both core and access network segments, upon the technological readiness of optical transceivers, optical fibers, amplifiers, filters, and other passive/active elements. Nowadays fiber-optic communication networks are wrapping around the globe, serving as the backbone of our information-driven society. Inside an optical network, regardless of its range or topology, every optical link requires a pair of optical transceivers with semiconductor lasers inside. These lasers, either directly modulated or externally modulated, have directly impacted the evolution of the telecom and datacom industry until today.

On the wireless communications side, the microwave technologies, which have established a strong momentum from their long-term development and heavy investment up to now, have managed to fulfill the requirements of the initial phase of 5G infrastructure that is currently under deployment. However, the microwave-based solutions, millimeter-wave (mmWave) included, are reaching their upper physical limit in supporting higher bandwidth for future applications beyond the current generation. Subsequently, higher frequency bands, such as the terahertz (THz) band and the mid-IR band, spanning a much broader range in the electromagnetic spectrum, appear as promising candidates to unlock such limitations.[1,2] There have been several experimental demonstrations with high data rate transmissions in the THz band, many of them assisted with photonic technologies.[3–5] On the other hand, along with the upshifted carrier frequency and broadened bandwidth, these wireless systems are adopting a new paradigm where the signals are emitted as guided waves with high-gain

Dr. X. Pang, Dr. O. Ozolins, Dr. R. Schatz, Prof. S. Popov,
Prof. S. Lourdudoss
Department of Applied Physics
KTH Royal Institute of Technology
Stockholm 10691, Sweden
E-mail: xiaodan@kth.se

Dr. O. Ozolins, Dr. A. Udalcovs, Prof. G. Jacobsen
Networks unit
RISE Research Institutes of Sweden
Kista 16440, Sweden

Dr. L. Zhang, Prof. X. Yu
College of Information Science and Electronic Engineering
Zhejiang University
Hangzhou 310027, China

Dr. L. Zhang, Prof. X. Yu
Zhejiang Lab
Hangzhou 310000, China

Prof. J. Chen
Department of Electrical Engineering
Chalmers University of Technology
Gothenburg 41296, Sweden

antennas or antenna arrays instead of being broadcasted as in the low-frequency bands; thus, high directivity is no longer considered as a drawback. Such a new paradigm resembles the properties of free-space optical communications (FSOC) that have been used for fixed links in the open air. Therefore, it attracts renewed interest to investigate whether optical technologies can be adopted in such application scenarios as the THz technologies.

There are several transmission windows applicable for FSOC with lower propagation loss, including the 0.8 μm band in the NIR, the 1.55 μm band in the short-wavelength IR (SWIR), the 4.5–5.2 μm band in the mid-wavelength IR (mid-IR), and the 8–12 μm band in the long-wavelength IR (LWIR).[6] Among these options, the 1.55 μm band, which is also referred to as the telecom band, is the commonly used band for commercial FSOC systems. This is mainly because of the maturity of active and passive components and devices driven by fiber optics. However, a major drawback is its very high sensitivity to atmospheric channel perturbations such as dust, fog, and turbulence. In such a context, the mid-IR and the LWIR bands are becoming options of interest due to their more stable performance through the atmospheric channel.[7,8] A recent study shows that the mid-IR FSOC link outperforms the 1.55 μm band during a 30 h operation in a foggy month.[9]

A feasible source to facilitate the benefits of the mid-IR is important. However, due to the mismatch in material bandgap, it is not straightforward to convert the semiconductor lasers used in fiber-optic transceivers to directly operate in the mid-IR. Several mid-IR FSOC demonstrations have been reported by using nonlinear frequency conversion between 1.55 μm and the mid-IR wavelength before and after the free-space link; in such a way the telecom band laser sources and detectors can be directly used, and high data rates are supported.[10–15] However, the high-power requirement and the large size of the nonlinear wavelength conversion modules hinder their practical applications. And in the long run, semiconductor lasers directly emitting at the desirable wavelength are favorable for compact FSOC transceivers. In this context, quantum cascade lasers (QCLs), which exploit the inter-subband transitions to cover the wavelength range from the mid-IR to the THz,[16,17] have shown great potential in acting as the light source that is to be integrated inside future mid-IR FSOC transceivers. Similarly to the directly modulated lasers in the telecom band, QCLs can be directly modulated with a high-speed digital signal. Moreover, QCLs benefit from their much shorter carrier relaxation lifetime than that of conventional semiconductor lasers, making the laser response overdamped without a resonance frequency and increasing the modulation bandwidth.[18,19] For example, a 26.5 GHz direct modulation of a mid-IR QCL of buried heterostructure was recently reported.[20] One can find a detailed review reported by Vitiello et al. on the development of QCL.[21] To date, there have been several experimental demonstrations using QCLs for FSOC across a broad wavelength range from the mid-IR to the THz band,[22–37] which are summarized in detail in the following section. Among these works, we have previously reported gigabit data transmissions with a directly modulated QCL at room temperature, where we achieved a 3 Gb s⁻¹ data rate with three different modulation formats, namely, non-return-to-zero (NRZ) on–off-keying (OOK) and 4- and 8-level pulse amplitude modulation (PAM-4 and PAM-8)

formats.[36] We also briefly presented our latest results in Pang et al.,[37] which will be elaborated in this study with detailed descriptions of operational principle and discussions on results. To effectively utilize the broad modulation bandwidth, high linearity, and large dynamic range (low noise level) of the directly modulated QCL, we converge our selection into two modulation formats, namely, PAM-4 and discrete multitone (DMT), and demonstrate successful modulation and reception of up to a 4 Gb s⁻¹ transmission data rate. Effective digital adaptive equalizers are shown to be a key enabling technique for both modulation formats.

The remaining study is organized as follows. In Section 2, we review the status of QCL-based FSOC systems that are experimentally demonstrated. Then in Section 3 we present the FSOC experimental setup with a 4.65 μm QCL and show the system-level channel characteristics. In Section 4, we show the experimental results for the two adopted modulation formats, respectively, and describe the equalization techniques in detail. Finally, we conclude our work and provide our perspectives on future efforts.

2. Summary of Reported QCL-Based FSOC Experiments

From the early 2000s, QCLs have already been considered for mid-IR and LWIR FSOC applications. Due to the lack of maturity in relevant devices and components in these frequencies, the progress in this field is lagging behind the FSOC development in the 1.55 μm telecom band. Nevertheless, the future 6G requirements reopen new opportunities for QCLs as new spectral windows become necessary for high-speed communications. In this section, we try to summarize the experimental works reported on QCL-based FSOC systems, aiming to provide an overall picture of the status in this research direction. It is noted that the FSOC demonstrations with interband cascade laser (ICL), though it is not technically a QCL, are included in this summary due to their similarities. Similar to the QCL in terms of using the concept of band structure engineering, the ICL is based on interband transitions mainly in Sb-based semiconductor heterostructures.[38] The ICL has demonstrated high performance with low power-consumption, while mostly confined in the 3–5 μm mid-IR region.[39]

Table 1 summarizes various FSOC experiments using a QCL or ICL as the transmitter source, and the key figures of merit from several aspects are listed, including the operational wavelength, the transmitted signal data rate or bandwidth, the modulation format used, the free-space channels that are evaluated in these experiments, and the laser operational temperature. To the best of our knowledge, the first experiment using a QCL for signal transmission was reported in 2001, where Martini et al. demonstrated a FSOC link across 70 m distance in an indoor environment. In this demonstration, a 7.3 μm QCL operated at a temperature of 80 K was modulated with a 10 MHz analog signal.[22] The same group later extended their results by first demonstrating up to 2.5 Gb s⁻¹ NRZ-OOK transmission over 1 m distance and later achieving an outdoor transmission of ≈100 m with a multichannel quadrature phase-shift-keying (QPSK) signal carrying ≈650 television channels at 8.4 μm.[23,24]

Table 1. List of experimental demonstrations of FSOC based on QCL/ICL.

Wavelength	Data rate/ bandwidth[a]	Modulation format	Channel	QCL operation temperature	Year	Ref. no.
7.3 μm	10 MHz[b]	Analog signal	70 m indoor	80 K	2001	[22]
8.1 μm	2.5 Gb s^{-1}	NRZ-OOK	1 m	85 K	2001	[23]
8.1 μm	750 MHz–1.5 GHz	Multichannel QPSK	100 m outdoor	25 K	2002	[24]
9.3 μm	330 MHz/115 kb s^{-1}	Analog/NRZ-OOK[c]	350 m outdoor/10 m indoor	258 K	2001	[25]
10.46 μm	20 kHz	Pulse frequency modulation	6000 m outdoor	240–340 K	2008	[26]
3 μm	70 Mb s^{-1}	NRZ-OOK	1 m	77 K	2009	[27]
73 μm	580 kHz	Analog signal	2 m	10 K	2011	[28]
72.6 μm	1 Mb s^{-1}	NRZ-OOK	2.2 m	13 K	2013	[29]
77 μm	5 Mb s^{-1}	NRZ-OOK	2.4 m	10 K	2013	[30]
92 μm	20 Mb s^{-1}	NRZ-OOK	2.2 m	11 K	2015	[31]
4.7 μm	40 MHz	Analog video signal	2.5 m	Room temperature[c]	2015	[32]
Mid-IR[d]	20 MHz	32-ary PPM	Turbulence simulator	Uncooled[c]	2015	[33,34]
10.6 μm	1 Gb s^{-1}	NRZ-OOK	Not specified	298 K	2019	[35]
4.65 μm	3 Gb s^{-1}	NRZ-OOK, PAM-4, PAM-8	5 cm	293 K	2017	[36]
4.65 μm	4 Gb s^{-1}	PAM-4, DMT	5 cm	293 K	2017	[37], this work

[a]The data rate for digital transmission and modulation bandwidth for analog transmission are listed, respectively; [b]Modulated on to a 66 MHz carrier; [c]Operation temperature not explicitly specified; [d]Wavelength not explicitly specified.

All these demonstrations required a QCL operated at cryogenic temperature. Around the same time, Blaser et al. reported room temperature operation of a 9.3 μm QCL at 258 K supporting both digital and analog signal transmissions in indoor and outdoor environments.[25] In 2008, an outdoor transmission over 6000 m with 20 kHz pulse frequency modulation was demonstrated by Taslakov et al. with a pulsed QCL operated at room temperature.[26] In 2010, Soibel et al. utilized an in-house-developed high-speed ICL at 3 μm to realize a up to 70 Mb s^{-1} mid-IR free-space transmission with a bit-error rate (BER) less than 10^{-8}.[27] After 2010, there were several reports of FSOC demonstrations with QCLs in the THz band, all operated at cryogenic temperature.[28–31] Other mid-IR transmissions at room temperature were also reported with different signal formats, although at low speed.[32–34] A recent report from the Combat Capabilities Development Command Army Research Laboratory (CCDC-ARL) introduced their plan on establishing an LWIR FSOC testbed based on 10.6 μm commercial off-the-shelf QCLs, indicating renewed interest in this research area.[35]

As we have previously mentioned, our recent experimental efforts in demonstrating multigigabit transmission with advanced modulation formats are included in the list in Table 1. More details on the experimental configuration and results are presented in the following sections. For others works, interested readers can refer to the original papers listed in Table 1 for more technical details. It is noted that the references listed previously are by no means exhaustive, and there might be more published literature in this area. Moreover, up to date the FSOC works that are summarized in this section are based on electrical modulation. Though it is predicted that the fundamental limit of the QCL modulation bandwidth can reach the scale of THz,[40] in practice the electrical modulation bandwidth is limited by the parasitic effects to maximally a few tens of gigahertz.

Moreover, optimized heat transport in recent QCL designs for high-power room-temperature operation typically worsen the parasitic issue, impose constraints on further increasing the modulation bandwidth. In this context, all-optical modulation methods have been proposed and studied, which avoid the electrical circuitry bottlenecks, providing an interesting alternative for the high-speed modulation of QCLs.[41–44]

3. Experimental Setup of a Mid-IR QCL-Based Free-space Transmission System

The experimental setup of the QCL-based FSOC system is shown in **Figure 1**. The QCL used in the measurements was a packaged distributed feedback (DFB) laser model from a previously reported design, which was fabricated by mirSense.[45] At room temperature, the QCL has a lasing threshold of 178 mA/10.7 V and a center wavelength of 4.65 μm, with a maximum continuous optical power of 60 mW at 350 mA driving current. The QCL was mounted on a commercial QCL mount (ILX Lightwave LDM-4872) and a water-cooled Peltier element was used to control the temperature at 20 °C. A custom-made bias tee was used to deliver the bias current and modulation signal to the QCL.[46]

Signals with different modulation formats were first generated offline in MATLAB as digital samples, before being converted to the analog domain by an arbitrary waveform generator (AWG) with a digital-to-analog converter (DAC) of 50 GSa s^{-1}. The AWG output was first amplified to around 1.3 Vpp before being combined with the laser bias to drive the QCL. At the output of the QCL, the modulated light beam at 4.65 μm was emitted into free space. As the emitted beam had a large divergence and a matched focusing lens was absent for this initial demonstration,
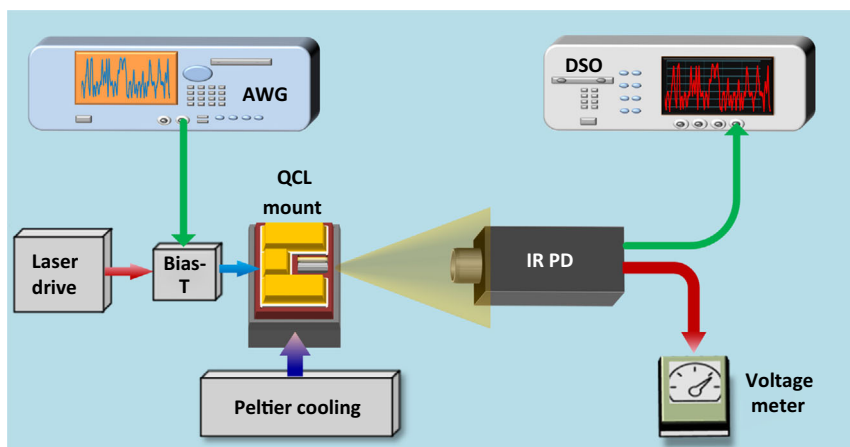
**ADVANCED
SCIENCE NEWS**

www.advancedsciencenews.com

**physica pssa
status
solidi**

www.pss-a.com

Figure 1. Experimental setup.

the distance between the infrared photodetector (IR PD) and the transmitter QCL was kept within 5 cm as a back-to-back scenario.

A commercial off-the-shelf $0.5\,\text{mm} \times 0.5\,\text{mm}$ IR PD (Vigo System SA) was used at the receiver side to collect the emitted signal. The IR PD with a built-in transimpedance amplifier (TIA) was mounted in a thermoelectrically cooled module. Per the manufacturer's specifications, it has an estimated 3 dB bandwidth of 720 MHz. A voltage meter was used to measure the photovoltage induced by the received signal at the PD, as shown in Figure 1, and a real-time digital storage oscilloscope (DSO) with an analog-to-digital converter (ADC) rate of $10\,\text{GSa}\,\text{s}^{-1}$ was used to sample and convert the electrical signal into the digital domain. The digitized waveforms were then sent back to a computer and processed offline. It is worth noting that the AWG and the DSO were connected to the same computer and controlled by the same script, which formed a closed loop and ran continuously to capture and process the received signal in a quasi-real-time manner.

The end-to-end channel frequency response of the QCL and the IR PD link was characterized with a vector network analyzer (VNA) and is shown in **Figure 2**. From the figure one can see that

the 3 dB system bandwidth was measured to be around 320 MHz. A three-pole model curve with a RC cutoff at 347 MHz and a damped resonance at 469 MHz can be used to fit the channel response, which results in $\approx$323 MHz, 3 dB bandwidth and 444 MHz, 6 dB bandwidth. It was also observed that the system bandwidth was virtually independent of the bias to the laser, and it was most likely limited by the electrical parasitic in the laser mount and the IR PD bandwidth. Thus, a higher-bandwidth detector and an improved mounting setup can potentially characterize the limits of the QCL module more accurately in the future.

4. Experimental Results

To upgrade the transmission data rate in bandwidth-limited systems, it has become a common practice to adopt advanced modulation formats of higher spectral efficiencies than the NRZ-OOK signal format. Among all feasible technical candidates, high-order PAM and DMT are two main options that have attracted most attention and are chosen for detailed experimental investigations using the system setup described previously.
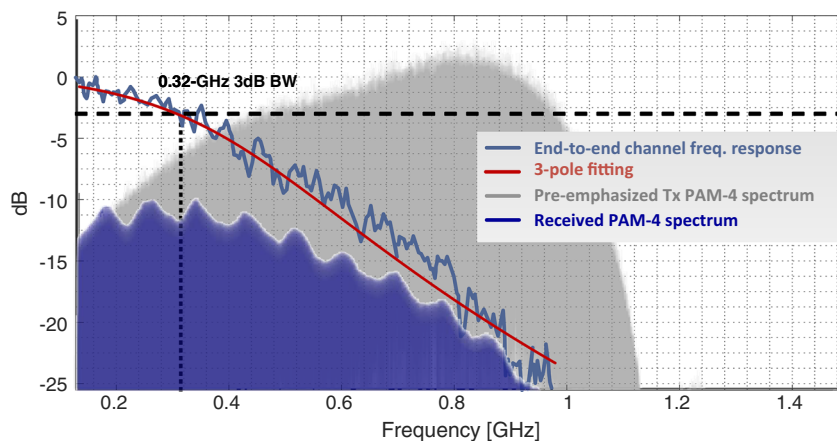

Figure 2. End to end channel frequency response with a fitting curve of a three-pole model, and the spectra of the transmitted and received PAM-4 signal, respectively. The PAM-4 signal shown in this figure is $4\,\text{Gb}\,\text{s}^{-1}$ with pulse shaping of 0.2 roll-off factor.

4.1. PAM-4

A PAM signal encodes binary data into multiple amplitude levels, and the conventional NRZ-OOK is its simplest 2-level form. Using a PAM signal with more amplitude levels results in a higher system spectral efficiency. However, for an N-level PAM signal the eye height for each level is reduced by a factor of $(N-1)$ (PAM-N, $N>2$) and compared with that of NRZ-OOK of the same peak-to-peak amplitude, and it requires a higher system signal-to-noise ratio (SNR). In addition, more amplitude levels require higher system linearity for modulation and demodulation. We have previously shown that the QCL under test has a high linearity to support up to 8-level PAM signaling at lower rate.[36] In this study, considering the trade-off between system SNR and bandwidth, PAM-4 is selected for detailed transmission performance evaluation.

With the increase in signal amplitude levels, it becomes extremely challenging to achieve "error-free" transmission using the NRZ-OOK. A common practice is to use digital pre- and postequalization techniques combined with forward-error correction (FEC) codes to reach a satisfying BER level fulfilling the application requirements. Two commonly used equalizer structures for PAM signals are the feedforward equalizer (FFE) and decision-feedback equalizer (DFE).[47]

Figure 3 shows the digital signal processing routine used in this experiment at both the transmitter and the receiver for the PAM-4 generation and reception. The transmitted data are a pseudorandom bit sequence of length $2^{15}-1$ (PRBS-15), which was mapped into PAM-4 symbols. The PAM-4 symbols were upsampled and pulse shaped by a root-raised-cosine filter. The waveforms were then resampled to match the AWG sampling rate. Due to the bandwidth limitation and frequency roll-off from the laser mount and the commercial IR PD, the transmitted signal was pre-equalized by a static 2-tap pre-emphasis filter. Figure 2 shows the 2 Gbaud PAM-4 spectra both at the transmitter and the receiver. One can see that the transmitter-side pre-equalization lowers the SNR of the transmitted signal at low frequencies. At the receiver, the digital signals were matched filtered and resampled to four samples per symbol for timing recovery. The detailed timing recovery algorithm that performs sample selection can be found in a previous study.[48] After the timing recovery, the signals were downsampled to one sample per symbol before being equalized by the FFE or DFE.
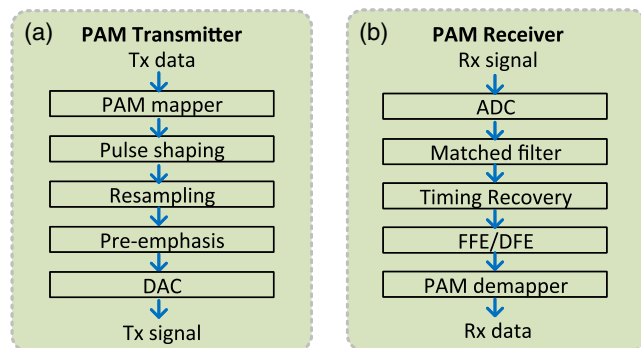
Figure 4 shows the transmission performance of the PAM-4 signal at $4\,\mathrm{Gb\,s^{-1}}$ over the QCL-based mid-IR system. We first evaluate the impact of the roll-off factors of the transmitter pulse-shaping filter. Figure 4 a shows the BER curves as a function of the received photovoltage measured with the voltage meter, which linearly reflects the received optical power at the IR PD. It is noted that the IR PD has a static photovoltage offset of $-1.016\,\mathrm{V}$ without any input signal. Three values of roll-off factors, namely, 0.1, 0.15, and 0.2, are evaluated with two post-equalization configurations, respectively. A roll-off factor of 0.2 appears to be the optimal option among the three tested cases as shown in the figure, and further increase of this value resulted in a performance degradation due to the limited system bandwidth. Figure 4b shows the pre-FEC BER results of different equalizer configurations with a fixed pulse shaping roll-off of 0.2. An FFE with different feedforward-tap (FWT) numbers ranging from 3 to 33 was tested in our experiment, while a DFE with the same number of FWTs plus three feedback taps (FBTs) was also used for comparison. For the FFE with FWTs only, it was observed that 13 taps are enough to achieve a BER performance below the 7% overhead hard decision FEC (7% OH HD FEC) limit of 3.8×10^{-3}, which then can be considered as "error free" after the FEC decoding. And the performance saturates with further increase of the tap numbers. In the case of the DFE, a 7-FWT and 3-FBT configuration was found sufficient to bring the BER performance below the 7% OH HD FEC limit. And in most cases with more than seven FWTs, with additional three FBTs the BER performance can be improved by approximately one order of magnitude. The corresponding eye diagrams of the unequalized signal, the signal after 13-FWT FFE, and the signal after the DFE with 13 FWT plus 3 FBT are shown in Figure 4c–e, respectively. One can clearly see that digital equalizers are necessary to achieve satisfying transmission performance at this baud rate, and the use of the DFE further opens the eye diagram compared with the case using the FFE only.

4.2. DMT

DMT is a type of frequency division multiplexing (FDM) modulation format, where the input data sequence is encoded in parallel onto many subcarriers (SCs).[49] Different from the single carrier signal formats, the DMT transmitter translates the serial input data sequence into parallel data streams and utilizes inverse fast Fourier transform (IFFT) to encode them into SCs in the frequency domain. A cyclic prefix (CP) is normally added to eliminate the intersymbol interference (ISI) and pilot symbols can be inserted to perform channel estimation. Recently, DMT has attracted attention for high-speed optical interconnects because of its flexibility to shape the signal spectrum to optimize the spectral efficiency through colored channels by using bit-/power-loading schemes. Unlike the PAM-4, pre- or postequalization for DMT is not performed with the target of flattening the received signal spectrum by suppressing the low-frequency signal components. Instead, a probe signal is first sent through the channel to estimate the channel response and calculate the in-band frequency-dependent SNR values, and then modulation orders and power levels for each SC are assigned accordingly in the DMT signal. A widely adopted bit-/power-loading approach is
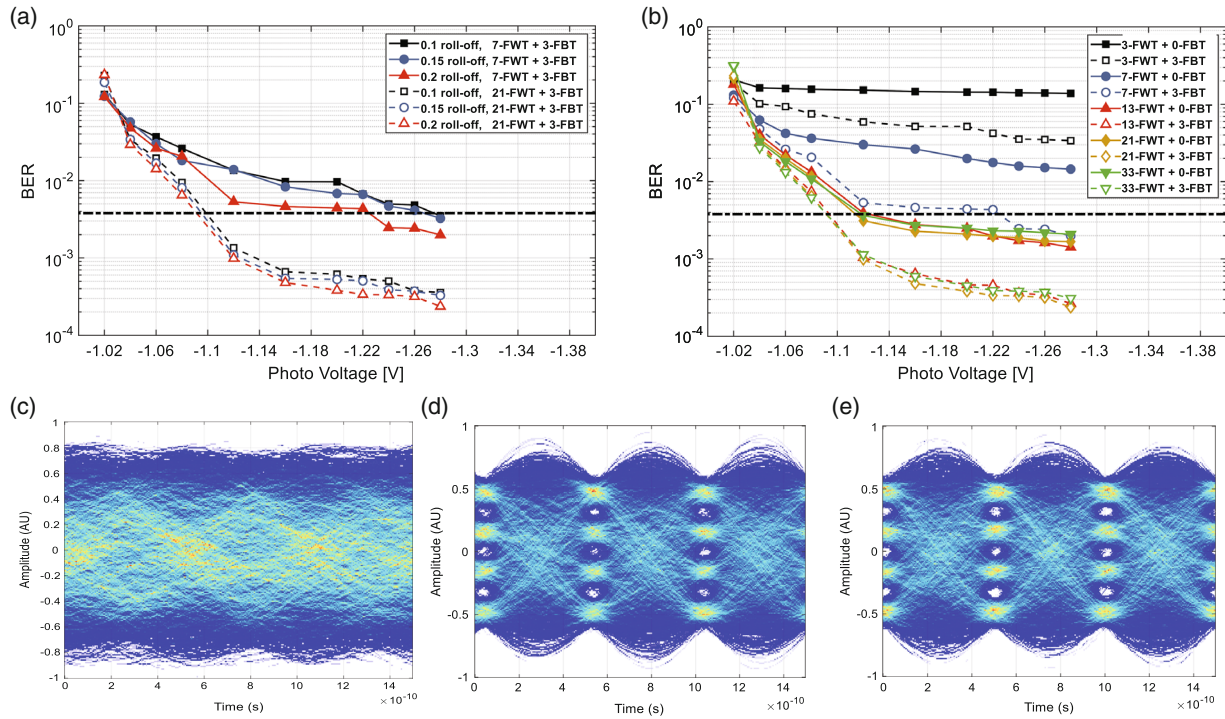

Figure 3. DSP routine of the PAM-4 transmitter and receiver. a) transmitter and b) receiver.

ADVANCED
SCIENCE NEWS
www.advancedsciencenews.com

physica
pss status solidi a
www.pss-a.com

Figure 4. Transmission performance of the PAM-4 signal at 4 Gb s^{-1}. a) BER evaluation of the impact of the signal pulse-shaping roll-off factors (three cases: 0.1, 0.15, and 0.2). b) BER results of different FFE (solid lines)/DFE (dashed lines) configurations with 0.2 roll-off pulse shaping. Eye diagrams of c) unequalized received signal, d) received signal equalized with 13-FWT FFE, and e) received signal equalized with 13-FWT + 3-FBT DFE.

known as Chow's algorithm,[50] which was used in our FSOC experiment. Although the overall channel utilization efficiency is improved, a major drawback of DMT is the high peak-to-average power ratio (PAPR). A performance trade-off between spectral granularity of the DMT SCs and system linearity thus exists. Moreover, compared with PAM-4, the DMT signal with a high PAPR shows a lower tolerance to the relative intensity noise (RIN) of lasers.[51]

Figure 5 shows the digital signal processing routine used in this experiment at both the transmitter and the receiver for the generation and reception of the DMT signal. We used an IFFT of length 32 768 and a CP of 512, respectively, which were fixed for all cases. The high IFFT number is used to avoid the AWG

aliasing effect at high sampling rate. After the IFFT, to avoid DC leakage, the first eight SCs are set to null. With the target of maximizing the overall data rate, different SC modulation orders and effective SCs numbers, as well as a water-filling scheme with bit/power loading, are tested and evaluated. At the receiver, after synchronization and CP removal, we use a frequency domain linear equalizer for channel equalization. Finally, the equalized signal is demapped to bit-sequence and evaluated for BER performance.

Four different SC constellation schemes are evaluated. In the first three schemes, we select three typical modulation formats, namely, the 16-ary quadrature amplitude modulation (QAM), 64QAM, and 128QAM. In these three cases, the same modulation
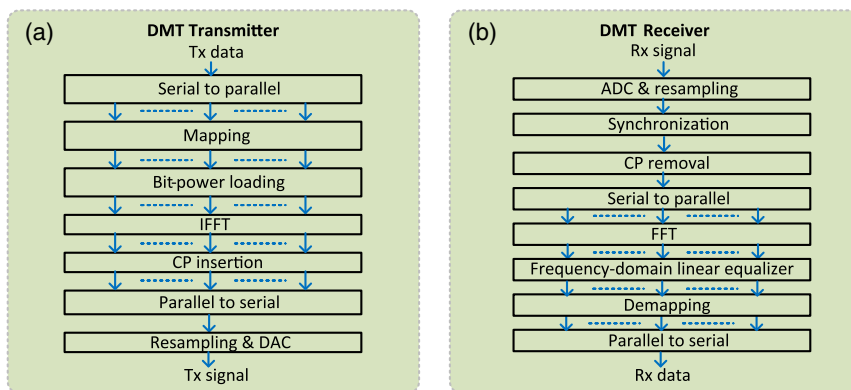

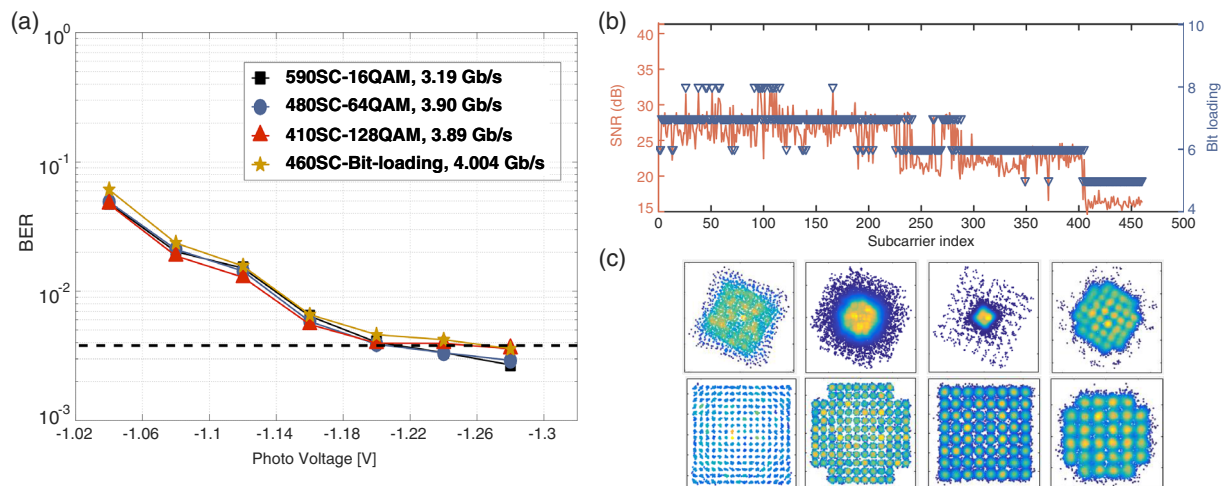**Figure 5.** DSP routine of a) the DMT transmitter and b) the DMT receiver.

Figure 6. Transmission performance of the DMT signals. a) BER performance of DMT with different SC modulations. b) The probed SNR values across the SCs and the bit allocation for the SC bit-loading scheme with Chow's algorithm. c) Corresponding SC constellations with different modulation orders before the channel equalization (upper row) and after the channel equalization (bottom row).

orders are applied across all SCs. Due to the differences in the required SNR, different numbers of SCs are used for different modulation orders, resulting in different data rates. In the case of the 16QAM, 590 SCs are used and a pre-FEC data rate of $3.19\,\mathrm{Gb\,s^{-1}}$ is achieved. For the 64QAM and the 128QAM, 480 used SCs with a data rate of $3.90\,\mathrm{Gb\,s^{-1}}$ and 410 used SCs at $3.89\,\mathrm{Gb\,s^{-1}}$ are achieved, respectively. The pre-FEC data rate is calculated by subtracting the CP length and the pilot symbols from the overall transmitted signal. And the fourth scheme utilizes the bit-loading scheme with different modulation orders for SCs with different SNRs (460 SCs, $4.004\,\mathrm{Gb\,s^{-1}}$ pre-FEC data rate). **Figure 6**a shows the BER performance of the DMT signals with the four SC constellation allocation schemes. As the number of effective SCs and the net transmitted data rates were chosen with a target of below the 7% OH HD FEC limit, the BER performance of all four cases satisfies the "error free" criterion. The SC SNR and bit allocations for the bit-loading scheme are shown in Figure 6b. It is noted that the eight null SCs are excluded in this figure and only the modulated SCs are shown. It is seen that the channel frequency response can be effectively utilized with high granularity using the corresponding bit allocation scheme and up to 256 QAM orders ($8\,\mathrm{bit\,symbol^{-1}}$) are supported in certain SCs with high SNR. Figure 6c also shows the corresponding constellations before and after the frequency domain linear equalizer, indicating the necessity of channel equalization.

As a final remark of the experimental evaluation of both modulation formats, we found that the PAM-4 transceivers are potentially simpler to implement as they resemble the conventional binary transceiver, only with increased amplitude levels. However, in a band-limited system such as our experimental setup, it requires pronounced pre-emphasis and postequalization of a long memory length, which translates into circuit complexity and power consumption. On the other hand, the DMT may require additional hardware modules for the FFT and IFFT process, but it shows a more flexible accommodation of the colored frequency channel and it is naturally suitable for frequency domain equalization. Therefore, both the modulation

formats should be considered for further research and development effort toward practical implementation, depending on the specific system requirements.

5. Conclusion

We made an overview of the status of QCL-based FSOC research and summarized the representative experimental demonstrations of such systems up to now. Our recent experimental investigations with advanced modulation formats are also presented in detail, and we show up to $4\,\mathrm{Gb\,s^{-1}}$ back-to-back connection with a directly modulated $4.65\,\mu\mathrm{m}$ QCL at room temperature. Two different modulation formats, PAM-4 and DMT, are evaluated with this setup. Compared with other FSOC systems, particularly the ones operating in the $1.55\,\mu\mathrm{m}$ telecom band, the technology readiness level of the QCL-based approach is still far behind. However, it is believed that continued research effort in this direction can be rewarding, as there is great application potential contained in the mid-IR and LWIR FSOC systems for the future 6G era. Future research steps include the use of a quantum cascade detector with coherent reception to further increase the system capacity with longer transmission distance. Moreover, different multiplexing schemes such as wavelength-division multiplexing (WDM) and spatial multiple-input multiple-output (MIMO) technologies should be investigated for the untapped spectral resources in the mid-IR and LWIR. Finally, based on specific use cases and application scenarios, performance comparisons and potential complementary convergence between the QCL-based FSOC and other free-space communication approaches, for instance, the THz systems, should be investigated.

Acknowledgements

no. 828893, and in part by the ERDF-funded CARAT project (1.1.1.2/VIAA/4/20/0xx). This work made use of facilities in KTH/RISE shared Kista High Speed Transmission Lab and equipment sponsored by the Knut and Alice Wallenberg foundation. The authors would like to acknowledge the support of Gregory Maisons and Mathieu Carras from mirSense for providing the mid-IR QCL module and thank Joakim Storck for mounting and characterizing the QCL.

Conflict of Interest

The authors declare no conflict of interest.

Keywords

[1] M. Giordani, M. Polese, M. Mezzavilla, S. Rangan, M. Zorzi, *IEEE Commun. Mag.* **2020**, *58*, 55.
[2] Z. Zhang, Y. Xiao, Z. Ma, M. Xiao, Z. Ding, X. Lei, G. K. Karagiannidis, P. Fan, *IEEE Veh. Technol. Mag.* **2019**, *14*, 28.
[3] T. Nagatsuma, G. Ducournau, C. C Renaud, *Nat. Photonics* **2016**, *10*, 371.
[4] S. Jia, X. Pang, O. Ozolins, X. Yu, H. Hu, J. Yu, P. Guan, F. Da Ros, S. Popov, G. Jacobsen, M. Galili, T. Morioka, D. Zibar, L. K. Oxenløwe, *J. Lightwave Technol.* **2018**, *36*, 610.
[5] X. Pang, S. Jia, O. Ozolins, X. Yu, H. Hu, L. Marcon, P. Guan, F. Da Ros, S. Popov, G. Jacobsen, M. Galili, T. Morioka, D. Zibar, L. K. Oxenløwe, in *IEEE Photonics Conf.*, IEEE, Waikoloa, HI **2016**.
[6] H. Henniger, O. Wilfert, *Radioengineering* **2010**, *19*, 2.
[7] T. Plank, E. Leitgeb, P. Pezzei, Z. Ghassemlooy, in *17th European Conf. Networks and Optical Communications*, IEEE, Gothenburg **2012**, pp. 1–5.
[8] A. Delga, L. Leviandier, *Proc. SPIE* **2019**, *10926*, 1092617.
[9] C. Sauvage, C. Robert, B. Sorrente, F. Grillot, D. Erasme, in *Environmental Effects on Light Propagation and Adaptive Systems II*, SPIE, Strasbourg, Vol. *11153*, **2019** p. 111530I.
[10] E. Ip, D. Büchter, C. Langrock, J. M. Kahn, H. Herrmann, W. Sohler, M. M. Fejer, in *European Conf. Optical Communication*, IEEE, Brussels **2008**, p. Tu.3.E.7.
[11] K. D. Büchter, H. Herrmann, C. Langrock, M. M. Fejer, W. Sohler, *Opt. Lett.* **2009**, *34*, 470.
[12] P. Cho, G. Harston, K. Büchter, D. Soreide, J. Saint Clair, W. Sohler, Y. Achiam, I. Shpantzer, *Proc. SPIE* **2009**, *7324*, 73240A.
[13] Q. Hao, G. Zhu, S. Yang, K. Yang, T. Duan, X. Xie, K. Huang, H. Zeng, *Appl. Opt.* **2017**, *56*, 2260.
[14] Y. Su, W. Wang, X. Hu, H. Hu, X. Huang, Y. Wang, J. Si, X. Xie, B. Han, H. Feng, Q. Hao, *Opt. Express* **2018**, *26*, 34515.
[15] W. Wang, Y. Zheng, X. Xie, Y. Su, X. Huang, T. Duan, W. Zhao, *Opt. Commun.* **2020**, 125681.
[16] R. F. Kazarinov, R. A. Suris, *Semiconductors* **1971**, *5*, 707.
[17] J. Faist, F. Capasso, D. L. Sivco, C. Sirtori, A. L. Hutchinson, A. Y. Cho, *Science* **1994**, *264*, 553.
[18] F. Capasso, R. Paiella, R. Martini, R. Colombelli, C. Gmachl, T. L. Myers, M. S. Taubman, R. M. Williams, C. G. Bethea, K. Unterrainer, H. Y. Hwang, D. L. Sivco, A. Y. Cho,

[19] A. M. Sergent, H. C. Liu, E. A. Whittaker, *IEEE J. Quantum Electron.* **2002**, *38*, 511.
[20] Y. Zhou, S. Zhai, J. Liu, F. Liu, J. Zhang, N. Zhuo, L. Wang, Z. Wang, *Electron. Lett.* **2016**, *52*, 548.
[21] M. Vitiello, G. Scalari, B. Williams, P. De Natale, *Opt. Express* **2015**, *23*, 5167.
[22] R. Martini, R. Paiella, C. Gmachl, F. Capasso, E. A. Whittaker, H. C. Liu, H. Y. Hwang, D. L. Sivco, J. N. Baillargeon, A. Y. Cho, *Electron. Lett.* **2001**, *37*, 1290.
[23] R. Martini, C. Gmachl, J. Falciglia, F. G. Curti, C. G. Bethea, F. Capasso, E. Whittaker, R. Paiella, A. Tredicucci, A. Hutchinson, D. L. Sivco, A. Y. Cho, *Electron. Lett.* **2001**, *37*, 191.
[24] R. Martini, C. Bethea, E Capasso, C. Gmachl, R. Paiella, E. A. Whittaker, H. Y. Hwang, D. L. Sivco, J. N. Baillargeon, A. Y. Cho, *Electron. Lett.* **2002**, *38*, 4.
[25] S. Blaser, D. Hofstetter, M. Beck, J. Faist, *Electron. Lett.* **2001**, *37*, 778.
[26] M. Taslakov, V. Simeonov, V. H. Van den Bergh, in *Free-Space Laser Communication Technologies XX,* Vol. *6877*, **2008**, p. 68770F.
[27] A. Soibel, M. W. Wright, W. H. Farr, S. A. Keo, C. J. Hill, R. Q. Yang, H. C. Liu, *IEEE Photon. Technol. Lett.* **2009**, *22*, 121.
[28] Z. Chen, Z. Y. Tan, Y. J. Han, R. Zhang, X. G. Guo, H. Li, J. C. Cao, H. C. Liu, *Electron. Lett.* **2011**, *47*, 1002.
[29] Z. Tan, Z. Chen, J. Cao, H. Liu, *Chin. Opt. Lett.* **2013**, *11*, 031403.
[30] Z. Chen, L. Gu, Z. Tan, C. Wang, J. Cao, *Chin. Opt. Lett.* **2013**, *11*, 112001.
[31] L. Gu, Z. Tan, Q. Wu, C. Wang, J. Cao, *Chin. Opt. Lett.* **2015**, *13*, 081402.
[32] C. Liu, S. Zhai, J. Zhang, Y. Zhou, Z. Jia, F. Liu, Z. Wang, *J. Semicond.* **2015**, *36*, 094009.
[33] E. Luzhansky, F. Choa, S. Merritt, A. Yu, M. Krainak, *Proc. SPIE* **2015**, *9465*, 946512.
[34] E. Luzhansky, F. Choa, S. Merritt, A. Yu, M. Krainak, *Imag. Appl. Opt.* **2015**, JT5A.7.
[35] J. J. Liu, B. L. Stann, K. K. Klett, P. S. Cho, P. M. Pellegrino, *Proc. SPIE* **2019**, *11133*, 1113302.
[36] X. Pang, O. Ozolins, R. Schatz, J. Storck, A. Udalcovs, J. Rodrigo Navarro, A. Kakkar, G. Maisons, M. Carras, G. Jacobsen, S. Popov, S. Lourdudoss, *Opt. Lett.* **2017**, *42*, 3646.
[37] X. Pang, O. Ozolins, L. Zhang, R. Schatz, A. Udalcovs, J. Storck, G. Maisons, M. Carras, S. Xiao, G. Jacobsen, S. Popov, J. Chen, S. Lourdudoss, in *European Conf. Optical Communication*, IEEE, Gothenburg **2017**, p. P2.SC6.31.
[38] R. Q. Yang, *Superlattices Microstruct.* **1995**, *17*, 77.
[39] A. Soibel, M. W. Wright, W. Farr, S. Keo, C. Hill, R. Q. Yang, H. C. Liu, *Electron. Lett.* **2009**, *45*, 264.
[40] N. Mustafa, L. Pesquera, C. Y. L. Cheung, K. A. Shore, *IEEE Photonics Technol. Lett.* **1999**, *11*, 527.
[41] C. Zervos, M. D. Frogley, C. C Phillips, D. O. Kundys, L. R. Wilson, M. Hopkinson, M. S. Skolnick, *Appl. Phys. Lett.* **2007**, *90*, 053503.
[42] G. Chen, C. G. Bethea, R. Martini, P. Grant, R. Dudek, H. Liu, *Appl. Phys. Lett.* **2010**, *95*, 101104.
[43] O. Spitz, A. Herdt, M. Carras, W. Elsässer, F. Grillot, in *Conf. Lasers and Electro-Optics*, OSA, San Jose, CA **2019**, p. SW3N.2.
[44] M. Montesinos-Ballester, V. Vakarin, J. M. Ramirez, Q. Liu, C. Alonso-Ramos, X. Le Roux, J. Frigerio, A. Ballabio, A. Barzaghi, L. Deniel, D. Bouville, L. Vivien, G. Isella, D. Marris-Morini, *Commun. Mater.* **2020**, *1*, 1.
[45] M. Carras, G. Maisons, B. Simozrag, M. Garcia, O. Parillaud, J. Massies, X. Marcadet, *Appl. Phys. Lett.* **2010**, *96*, 161105.
[46] J. Storck, *Master Degree Thesis*, KTH Royal Institute of Technology, Stockholm, Sweden, **2016**.

[47] J. G. Proakis, *Digital Communications*, Fourth Ed., McGraw-Hill, New York **2001**.

[48] A. Kakkar, J. Rodrigo Navarro, X. Pang, O. Ozolins, R. Schatz, U. Westergren, G. Jacobsen, S. Popov, in *The Optical Fiber Communication Conf. and Exhibition*, OSA, Los Angeles, CA **2017**, p. W2A.54.

[49] J. A. C. Bingham, *IEEE Commun. Mag.* **1990**, *28*, 5.

[50] P. Chow, J. M. Cioffi, J. A. C. Bingham, *IEEE Trans. Commun.*, **1995**, *43*, 773.

[51] H. Ochiai, H. Imai, *IEEE Trans. Commun.* **2001**, *49*, 282.

Xiaodan Pang is currently working as a senior researcher in the Department of Applied Physics, KTH Royal Institute of Technology, Sweden, from March 2020. He is/has been the PI of a Swedish Research Council Starting Grant, the EU H2020 Marie Curie Individual Fellowship Project NEWMAN, and a Swedish SRA ICT-TNG Post Doc project. His research focuses on ultrafast communications with mmW, THz, free-space optics, and fiber optics.